

# Self-Supervised Pre-Training for Precipitation Post-Processor

**Sojung An<sup>\*†</sup>**  
KIAPS  
Seoul, Republic of Korea  
sojungan@kiaps.org

**Junha Lee<sup>\*</sup>**  
KITECH  
Ansan, Republic of Korea  
junha@kitech.re.kr

**Jiyeon Jang**  
KIAPS  
Seoul, Republic of Korea  
jyjang@kiaps.org

**Inchae Na**  
KIAPS  
Seoul, Republic of Korea  
icna@kiaps.org

**Wooyeon Park**  
KIAPS  
Seoul, Republic of Korea  
wooyeon@kiaps.org

**Sujeong You**  
KITECH  
Ansan, Republic of Korea  
sjyou21@kitech.re.kr

## Abstract

Obtaining a sufficient forecast lead time for local precipitation is essential in preventing hazardous weather events. Global warming-induced climate change increases the challenge of accurately predicting severe precipitation events, such as heavy rainfall. In this paper, we propose a deep learning-based precipitation post-processor for numerical weather prediction (NWP) models. The precipitation post-processor consists of (i) employing self-supervised pre-training, where the parameters of the encoder are pre-trained on the reconstruction of the masked variables of the atmospheric physics domain; and (ii) conducting transfer learning on precipitation segmentation tasks (the target domain) from the pre-trained encoder. In addition, we introduced a heuristic labeling approach to effectively train class-imbalanced datasets. Our experiments on precipitation correction for regional NWP show that the proposed method outperforms other approaches.

## 1 Introduction

In modern society, precipitation forecasting plays a vital role in the response to and prevention of social and economic damage. Deep learning has been rapidly utilized in precipitation forecasting, such as for simulating echo movements and predicting typhoon trajectories based on observational data [20, 21, 17, 1]. However, exclusively relying on observational data fails to capture the fundamental physical and dynamic mechanisms in the real world. This results in an exponential increase in error as the forecast lead time increases [3]. In addition, climate change increases the uncertainty of predicting extreme events such as torrential rains [15]. A limited forecast lead time makes it difficult to prepare for extreme weather events in advance.

Recent research has been actively conducted to enhance forecast lead times via the post-processing of numerical weather prediction (NWP) model data [11, 6, 18, 25]. Espeholt et al. [3] proposed Metnet2, a 12-h probabilistic forecasting model. They designed a hybrid model consisting of a forecasting model based on observational data and post-processing NWP model data. While Metnet2 displayed promising results, simulating heavy rainfall remains a challenging task.

Therefore, we designed a self-supervised pre-training process that considers the physical and dynamic processes among atmospheric variables to improve the relative bias and reliability of predicting

<sup>\*</sup>These authors contributed equally to this work.

<sup>†</sup>Corresponding author

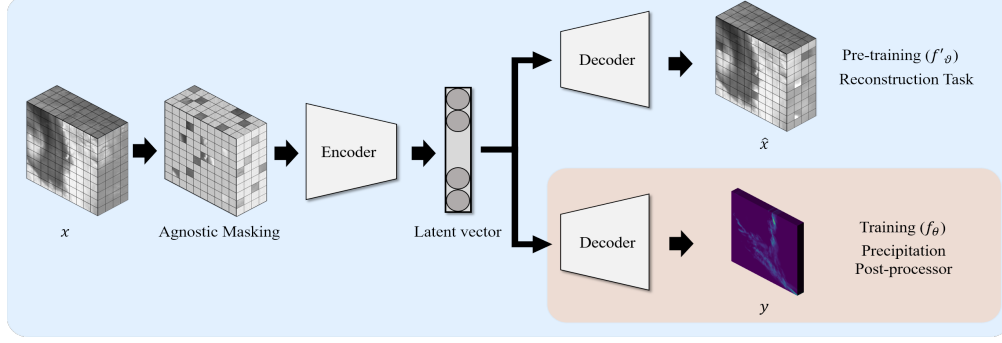


Figure 1: Process of learning the precipitation post-processor. The model consists of two main phases: 1) pre-training the encoder and decoder using a reconstruction task after masking the inputs and 2) training the decoder for precipitation prediction using the trained encoder. During the main training, the latent vector learned during pre-training is used as an encoder with fixed weights.

heavy rain. To this end, we randomly masked three-dimensional (3D) images [5] and trained an encoder-decoder to reconstruct variables based on dynamic sparse kernels (DSKs) [23]. Subsequently, we trained a decoder for probability-based precipitation correction based on a pre-trained encoder. The pre-training process helps in conducting a correlation analysis based on the NWP model variables and provides additional data-augmentation effects. Finally, we propose a continuous labeling method for learning class-imbalanced datasets. This method facilitates a continuous probability distribution based on the precipitation density.

## 2 Method

This section describes the proposed approach. We first present a self-supervised pre-training procedure that aims to define the reconstruction task. Subsequently, we describe the target process for the precipitation post-processing.

### 2.1 Problem formulation

Given a set of ground-truth pairs  $\mathbf{G} = (\{x_i\}_{i=1}^n, \{y_j\}_{j=1}^m)$  with  $x \in \mathbb{R}^{n \times h \times w}$ ,  $y \in \mathbb{R}^{m \times h \times w}$ , and  $z \in \mathbb{R}^d$ , let  $x = \{x_1, \dots, x_n\}^T$  represent the input, and  $y = \{y_1, \dots, y_m\}^T$  represent the output. Our objective is to derive a precipitation segmentation function  $f : \mathbb{R}^d \rightarrow \mathbb{R}^c$ , assuming  $z \in \mathbb{R}^d$  as a latent space with distribution  $p(z)$  defined by the pre-training process. The task involves reconstructing  $f'_\theta$  from the NWP data to predict the target object function  $f_\theta$ . The probabilistic encoder-decoder of the proposed method is defined as follows:

$$\mathcal{L}(\theta, \vartheta; x) = -\frac{1}{2} \mathbb{E}_{q_\vartheta(z|x)} [\|x - \hat{x}\|_2^2] + \text{KL}(q_\vartheta(z|x) \| p^*(y)), \quad (1)$$

where  $\hat{x}$  denotes the reconstructed output from  $x$  as generated by decoder,  $q_\vartheta$  represents the pre-training process distribution, and  $p^*$  is the class probability distribution, detailed in Section 2.2. The loss function combines the mean squared error for minimizing pre-training loss and the Kullback-Leibler (KL) divergence term to quantify the difference between the learned latent variable distribution  $q_\vartheta(z|x)$  and the class probability distribution  $p^*(y)$ .

### 2.2 Continuous labeling

In multi-class classification, instances  $x$  are classified into one of the  $y$  labels based on the ranges of precipitation intensity. Let  $p^*(y) = [\mathbb{P}(y|z)]$  be the class probability distribution and  $\mathcal{L}$  be the cross-entropy loss. For the predictive function  $f(x)$  and the label  $y$ , the cross-entropy loss  $\mathcal{L}(f(x), y)$  is computed as follows:

$$\mathcal{L}(f(x), y) = -\sum_{j=1}^m w_j \cdot p^*(y_j) \log(f(x)_j), \quad (2)$$

where  $w_j$  denotes the weight set according to each class label  $y_j$ , and  $p^*(\cdot)$  denotes the continuous labeling. The minimization leads to the maximum likelihood estimate of the classifier parameters. Minimization yields a maximum likelihood estimate of the classifier parameters. Algorithm 1 presents the method for smoothing the probability values based on the density of the label range. This method differs from that of one-hot labeling, where the probability takes a value of one. In the smoothing method, the sum of the probability values per class is fixed at one.

---

**Algorithm 1:** Continuous labeling of the density of the rainfall range

---

**Input:** QPE  $y = [0, 100]$ ; rainfall threshold set  $\gamma = \{r_0, \dots, r_{m-2}\}$ , ( $m \geq 2$ )

**Output:** Probability label  $p^*(y)$

```

1 Initialize the number of rainfall thresholds  $\gamma$ 
2  $p(y_j) = \begin{cases} 1, & \text{if } r_{j-1} \leq y < r_j \\ 0, & \text{otherwise} \end{cases}$  /* Set the probability of label  $k$  to 1. */
3 while  $j$  do
4   switch  $p(y_j)$  do
5     if  $\{x \leq r_{j-1}\}$   $p^*(y_j) \rightarrow 0$ 
6     else if  $\{r_{j-1} < y_j \leq r_j\}$   $p^*(y_j) \rightarrow 1 - \frac{y-r_j}{r_{j+1}-r_j}$ ,  $p^*(y_{j+1}) \rightarrow \frac{y-r_j}{r_j-r_{j-1}}$ 
7     else if  $\{j = m-2\}$   $p^*(y) \rightarrow 1$ 
8     else  $\Rightarrow p^*(y_j) \rightarrow 0$ 
9   end
10 end
11 return  $p^*(y)$ 

```

---

Given a rainfall  $y_c$  that lies between two thresholds  $r_{j-1}$  and  $r_j$ , assume that  $y_c$  is closer to  $r_j$ . The probability values for each threshold are sets  $p(y_{c=j}) = 1$  and  $p(y_{c \neq j}) = 0$ . In this context,  $p(\cdot)$  denotes the probability value based on the original labeling. According to Algorithm 1,  $p^*(y_{c+1})$  has a probability value of  $p^*(y_c) < p^*(y_{c+1})$ , and  $\sum p^*(y) = 1$ . Setting the probability value using one-hot labeling can be a limitation in learning the uncertainty of the NWP. By continuously smoothing the probability value of a label, the method can help reduce uncertainty about the likelihood of being a different label.

### 2.3 Training model

This section presents our post-processing method that perturbs an entire patch for the reconstruction task. This method uses InternImage [23] as an encoder and UPerNet [24] as a decoder.

**Patch embedding.** We tokenize the input data into nonoverlapping spatial-temporal patches [4]. Each 3D patch has dimensions  $\mathcal{M} \in \mathbb{R}^{t \times p \times p}$ , where  $t$  and  $p$  denote token size of time and height/width respectively. This patching approach results in  $x \in \mathbb{R}^{\frac{n}{t} \times \frac{h}{p} \times \frac{w}{p}}$  tokens. We then flatten the data and transform the tokens into  $x \in \mathbb{R}^{\frac{nhw}{4p^2} \times C}$  using a projection process. The data is added spatio-temporal positional encodings of the same size.

**Masking.** Based on reference [5], we use a structure-agnostic sample strategy to randomly mask the patches without using replacements from the set of embedded patches. For a pre-training model in a reconstruction task, the optimal masking ratio is related to the amount of redundant information in the data [2, 8]. Numerical forecasting models have a similar information redundancy, as each weather variable is at the same point in time. However, each variable has its own physical information. Based on this, we use empirical results to determine the masking ratio. The masking ratios of the pre-training and training are set to 90% and 25%, respectively. The masked patches underwent layer normalization and are restored to their original input dimensions of  $x' \in \mathbb{R}^{n \times h \times w}$ .

**Encoder and decoder.** We utilize DSK layers in the InternImage [23] encoder for adaptive spatial aggregation. InternImage is a backbone model that employs various techniques, in addition to attention, in the receptive field required for downstream tasks. InternImage applies each encoder layer  $e_i \subset e$  to a hierarchy of hidden states and the weights of each layer are stacked. We use the UPerNet decoder to enable effective segmentation while preserving object boundaries and details from the training data.

Table 1: Summary of results for our tasks.  $\mathcal{I}$ ,  $p^*$ , and  $\vartheta$  denote InternImage, label smoothing, and transfer learning, respectively. The tables compare the results of the models with thresholds of 0.1 and 10 mm.

Method	0.1 mm $\uparrow$				10 mm $\uparrow$			
	CSI	F1	Precision	Recall	CSI	F1	Precision	Recall
RDAPS	0.296	0.456	0.405	0.522	0.062	0.117	0.077	<b>0.238</b>
Metnet	0.276	0.433	0.427	0.439	0.007	0.015	0.015	0.274
Metnet+ $p^*$	0.271	0.427	0.390	0.472	0.057	0.107	0.002	0.275
$\mathcal{I}+p^*$	0.316	0.488	0.488	0.502	0.017	0.020	0.020	0.132
$\mathcal{I}+\vartheta$	0.329	0.443	0.443	<b>0.523</b>	0.060	0.076	0.075	0.222
$\mathcal{I}+p^*+\vartheta$ (ours)	<b>0.347</b>	<b>0.515</b>	<b>0.620</b>	0.481	<b>0.093</b>	<b>0.169</b>	<b>0.130</b>	0.227

### 3 Experiments

We classified rainfall up to  $[0, 0.1)$  as no rain,  $[0.1, 10)$  as rain, and above 10 as heavy rain. Figure 2 (a) shows the proportions of each label. The proportion of heavy rain within the training dataset was approximately 0.75%. This indicates a significant data imbalance. The class imbalance issue frequently observed in precipitation measurement data is a common challenge in precipitation forecasting. Therefore, we investigated how the proposed method addresses class imbalance issues during the model training process. We compared and evaluated our post-processor and heuristic label approaches with the state-of-the-art precipitation forecasting model called Metnet.

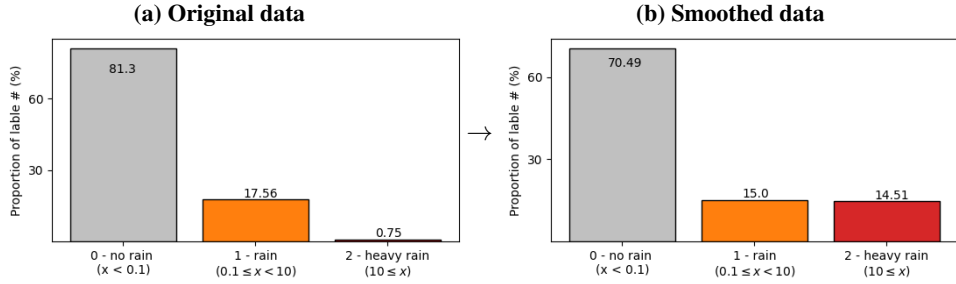


Figure 2: Visualization of the proportion of labels in the training dataset: (a) is the original data and (b) shows the proportion for pixels with a non-zero probability smoothed using the method proposed in Section 2.2.

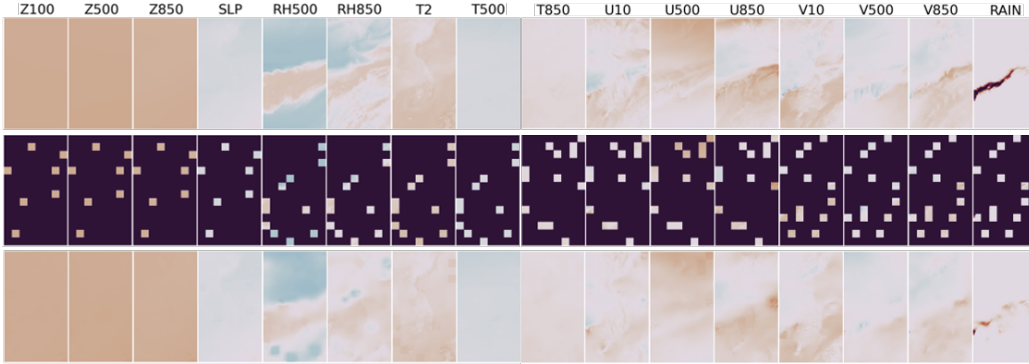


Figure 3: Variable reconstruction results using the pre-trained model on data from August 10, 2022 at 00 UTC. The first row visualizes the normalized variables. The second row visualizes the variables with 90% of the pixels masked. The third row shows the results of reconstructing the masked pixels. For the visualization, the masked values were set to -100, and a range of  $(-10, 10)$  was used. The number beside the variable indicates the vertical level.

Our main results are summarized in Table 1. For the pre-trained model, we used a mask ratio of 90%, a learning rate of  $1.6e-3$ , and approximately 150 k iterations. For the training model, we used a

mask ratio of 25%, a learning rate of  $1e-4$ , and approximately 35 k iterations. Training the model using continuous labeling had a noticeable impact on the performance improvement. We observed a significant enhancement in the accuracy of heavy rain when employing continuous labeling in Metnet. We aimed to address (i) solving the imbalanced label problem and (ii) learning the weights between the variables in the self-supervised learning.

Figure 3 shows the reconstruction of 16 masked variables. Using the pre-trained model to understand the physical flow based on changes in each variable and across vertical levels is crucial for precipitation prediction. Despite masking an overload of information in each variable, the NWP model accurately predicted prominent patterns across all variables. In particular, we observed a resemblance in the predicted patterns for the ‘rain’ variable despite the masked pixels carrying limited information for this instance and inherent nonlinearity of the variable.

Figure 4 shows that above 10 mm of precipitation covers much of the Korean Peninsula. A deep learning-based post-processing model captures above 10 mm of rainfall, while NWP models (RDAPS) underestimate this case. In Figure 4 (c), when trained with Algorithm 1, Metnet exhibits errors in the rainfall location but demonstrated accurate predictions for 10 mm of rainfall. In Figure 4 (d), for the proposed model, we observed predictions for rainfall location and 10 mm of rainfall, but these tended to be overestimated. Based on the results, combining  $p(y)$  and  $p^*(y)$  is expected to further enhance the accuracy. The limitation lies in the fact that the input data relies on NWP predictions. As a result, the prediction model learns with a certain margin of error and predicts in a manner similar to RDAPS in some cases.

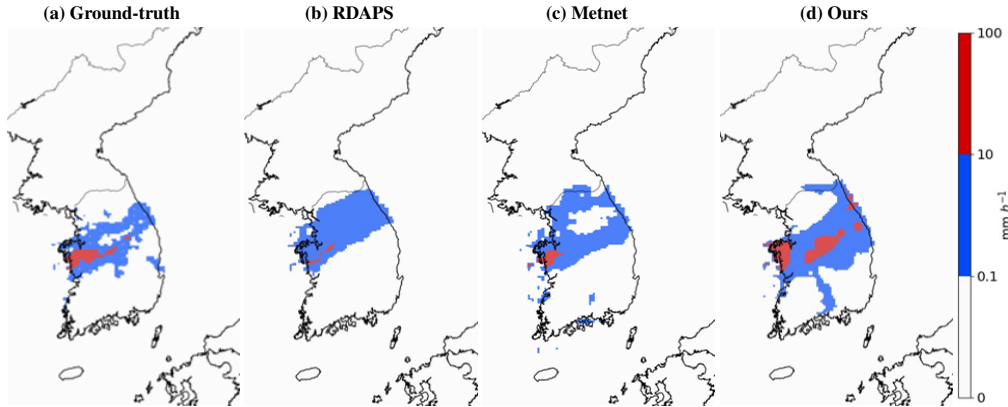


Figure 4: Qualitative comparison between models trained on data from August 10 2022 at 00 UTC. Each result represents a cumulative result over a 1-hour period. Owing to the influence of a stagnant front, rain fell in most parts of Korea; the average rainfall is 100~200 mm per day, and the maximum exceeds 300 mm.

## 4 Conclusion

This study proposes an approach for precipitation post-processing based on transfer learning for target domain adaptation. Our main contributions involve (1) applying transfer learning to the atmosphere system by conducting pre-training on the reconstruction domain and integrating the parameters in the segmentation domain and 2) employing stochastic softening one-hot labeling to overcome biased learning from unbalanced data. Our experiments on domain adaptation using the two-step training strategy show that the proposed method helps understand the correlation among atmospheric variables. This yields a better transfer learning performance from the precipitation post-processor.

## 5 Acknowledgments

This work was carried out through the R&D project “Development of a Next-Generation Operational System by the Korea Institute of Atmospheric Prediction Systems (KIAPS)”, funded by the Korea Meteorological Administration (KMA2020-02213).

## References

- [1] Sojung An. Nowcast-to-forecast: Token-based multiple remote sensing data fusion for precipitation forecast. In *Proceedings of the 32nd ACM International Conference on Information and Knowledge Management*, 2023.
- [2] Jacob Devlin, Ming-Wei Chang, Kenton Lee, and Kristina Toutanova. Bert: Pre-training of deep bidirectional transformers for language understanding. *arXiv preprint arXiv:1810.04805*, 2018.
- [3] Lasse Espeholt, Shreya Agrawal, Casper Sønderby, Manoj Kumar, Jonathan Heek, Carla Bromberg, Cenk Gazen, Rob Carver, Marcin Andrychowicz, Jason Hickey, et al. Deep learning for twelve hour precipitation forecasts. *Nature communications*, 13(1):1–10, 2022.
- [4] Haoqi Fan, Bo Xiong, Karttikeya Mangalam, Yanghao Li, Zhicheng Yan, Jitendra Malik, and Christoph Feichtenhofer. Multiscale vision transformers. In *Proceedings of the IEEE/CVF international conference on computer vision*, pages 6824–6835, 2021.
- [5] Christoph Feichtenhofer, Yanghao Li, Kaiming He, et al. Masked autoencoders as spatiotemporal learners. *Advances in neural information processing systems*, 35:35946–35958, 2022.
- [6] Mohammadvaghef Ghazvinian, Yu Zhang, Dong-Jun Seo, Minxue He, and Nelun Fernando. A novel hybrid artificial neural network-parametric scheme for postprocessing medium-range precipitation forecasts. *Advances in Water Resources*, 151:103907, 2021.
- [7] Priya Goyal, Piotr Dollár, Ross Girshick, Pieter Noordhuis, Lukasz Wesolowski, Aapo Kyrola, Andrew Tulloch, Yangqing Jia, and Kaiming He. Accurate, large minibatch sgd: Training imagenet in 1 hour. *arXiv preprint arXiv:1706.02677*, 2017.
- [8] Kaiming He, Xinlei Chen, Saining Xie, Yanghao Li, Piotr Dollár, and Ross Girshick. Masked autoencoders are scalable vision learners. In *Proceedings of the IEEE/CVF conference on computer vision and pattern recognition*, pages 16000–16009, 2022.
- [9] Ryan Keisler. Forecasting global weather with graph neural networks. *arXiv preprint arXiv:2202.07575*, 2022.
- [10] Ki-Hwan Kim, Pyoung-Seop Shim, and Seoleun Shin. An alternative bilinear interpolation method between spherical grids. *Atmosphere*, 10(3):123, 2019.
- [11] Taehyeon Kim, Namgyu Ho, Donggyu Kim, and Se-Young Yun. Benchmark dataset for precipitation forecasting by post-processing the numerical weather prediction. *arXiv preprint arXiv:2206.15241*, 2022.
- [12] Ilya Loshchilov and Frank Hutter. Sgdr: Stochastic gradient descent with warm restarts. *arXiv preprint arXiv:1608.03983*, 2016.
- [13] Ilya Loshchilov and Frank Hutter. Decoupled weight decay regularization. *arXiv preprint arXiv:1711.05101*, 2017.
- [14] Xin Man, Chenghong Zhang, Changyu Li, and Jie Shao. W-mae: Pre-trained weather model with masked autoencoder for multi-variable weather forecasting. *arXiv preprint arXiv:2304.08754*, 2023.
- [15] Katrin M Nissen and Uwe Ulbrich. Increasing frequencies and changing characteristics of heavy precipitation events threatening infrastructure in europe under climate change. *Natural Hazards and Earth System Sciences*, 17(7):1177–1190, 2017.
- [16] Jaideep Pathak, Shashank Subramanian, Peter Harrington, Sanjeev Raja, Ashesh Chattopadhyay, Morteza Mardani, Thorsten Kurth, David Hall, Zongyi Li, Kamyar Azizzadenesheli, et al. Fourcastnet: A global data-driven high-resolution weather model using adaptive fourier neural operators. *arXiv preprint arXiv:2202.11214*, 2022.
- [17] Suman Ravuri and Oriol Vinyals. Classification accuracy score for conditional generative models. *Advances in neural information processing systems*, 32, 2019.

- [18] Adrian Rojas-Campos, Martin Wittenbrink, Pascal Nieters, Erik J Schaffernicht, Jan D Keller, and Gordon Pipa. Postprocessing of nwp precipitation forecasts using deep learning. *Weather and Forecasting*, 38(3):487–497, 2023.
- [19] Ramprasaath R Selvaraju, Michael Cogswell, Abhishek Das, Ramakrishna Vedantam, Devi Parikh, and Dhruv Batra. Grad-cam: Visual explanations from deep networks via gradient-based localization. In *Proceedings of the IEEE international conference on computer vision*, pages 618–626, 2017.
- [20] Xingjian Shi, Zhouong Chen, Hao Wang, Dit-Yan Yeung, Wai-Kin Wong, and Wang-chun Woo. Convolutional lstm network: A machine learning approach for precipitation nowcasting. *Advances in neural information processing systems*, 28, 2015.
- [21] Xingjian Shi, Zhihan Gao, Leonard Lausen, Hao Wang, Dit-Yan Yeung, Wai-kin Wong, and Wang-chun Woo. Deep learning for precipitation nowcasting: A benchmark and a new model. *Advances in neural information processing systems*, 30, 2017.
- [22] Casper Kaae Sønderby, Lasse Espeholt, Jonathan Heek, Mostafa Dehghani, Avital Oliver, Tim Salimans, Shreya Agrawal, Jason Hickey, and Nal Kalchbrenner. Metnet: A neural weather model for precipitation forecasting. *arXiv preprint arXiv:2003.12140*, 2020.
- [23] Wenhai Wang, Jifeng Dai, Zhe Chen, Zhenhang Huang, Zhiqi Li, Xizhou Zhu, Xiaowei Hu, Tong Lu, Lewei Lu, Hongsheng Li, et al. Internimage: Exploring large-scale vision foundation models with deformable convolutions. In *Proceedings of the IEEE/CVF Conference on Computer Vision and Pattern Recognition*, pages 14408–14419, 2023.
- [24] Tete Xiao, Yingcheng Liu, Bolei Zhou, Yuning Jiang, and Jian Sun. Unified perceptual parsing for scene understanding. In *Proceedings of the European conference on computer vision (ECCV)*, pages 418–434, 2018.
- [25] Yuhang Zhang and Aizhong Ye. Machine learning for precipitation forecasts postprocessing: Multimodel comparison and experimental investigation. *Journal of Hydrometeorology*, 22(11): 3065–3085, 2021.
- [26] Bolei Zhou, Aditya Khosla, Agata Lapedriza, Aude Oliva, and Antonio Torralba. Learning deep features for discriminative localization. In *Proceedings of the IEEE conference on computer vision and pattern recognition*, pages 2921–2929, 2016.

## A Data

### A.1 RDAPS

In this study, we extracted data from the regional data assimilation and prediction system Korea integrated model (RDAPS-KIM) to obtain lead times from 25 to 30 h at 1-h intervals. The NWP models require approximately 6 h to generate a forecast field through data assimilation. Therefore, we extracted data from 25 to 30 h for a 24-h forecast. We organized the RDAPS-KIM into a domain with a resolution of 3 km. The domain covers the East Asia region. We set the variables based on previous studies [16, 14, 9], as shown in 2. The regional forecast model operates on a 6-h analysis-forecast cycle and utilizes hybrid sigma-pressure vertical coordinates with the Arakawa C-grid staggering grid system.

Table 2: Summary of datasets used as input data. This data consists of 16 variables. We used seven physical variables with four pressure levels: temperature (T),  $U$ -component of the wind speed (U),  $V$ -component of the wind speed (V), geopotential height (Z), relative humidity (RH), sea-level pressure (SLP), and rain.

Vertical Level	Variables
Surface	$U_{10}, V_{10}, T_2, SLP, rain$
850hPa	$U, V, T, Z, RH$
500hPa	$U, V, T, Z, RH$
100hPa	$Z$

### A.2 Ground-truth data

We used the quantitative precipitation estimation (QPE) dataset as the ground truth data. The QPE dataset is a reanalysis dataset for the Korean Peninsula. The data comprised data with a 5-km resolution at 1-h intervals and covered approximately a longitude of 149 to a latitude of 253. We adjusted the QPE data to the nearest natural rainfall by combining ground observations from AWS and SHK060, radar data, and satellite data.

## B Evaluating Metrics

For the verification, we used four standard evaluation metrics: the critical success index (CSI), F1 score, precision, and recall. The CSI was calculated as follows:  $CSI = \frac{TP}{TP+FP+FN}$ , where TP denotes the number of true positives, FP that of false positives, and FN that of false negatives between

$f_i^\theta$  and  $p_i^\theta$ .  $x^\theta$  is defined as zero or one according to a threshold  $x_i^\theta = \begin{cases} 1, & \text{if } x \geq \theta \\ 0, & \text{otherwise} \end{cases}$ . The CSI

is commonly used in precipitation forecasting tasks. It measures the number of correct forecasts divided by the number of occasions. The F1 score is a metric that combines the precision and recall to provide a single numerical value used to evaluate the performance of a classification model. The F1 score was computed as  $2 \times \frac{Precision \cdot Recall}{Precision + Recall}$ . Precision represents the percentage of correctly predicted positive samples and is calculated as  $\frac{TP}{TP+FP}$ . Recall is determined by dividing the number of hits by the sum of TPs and false FNs. Recall is calculated as  $\frac{TP}{TP+FN}$ .

## C Implementation

**Data pre-processing.** The data spanned from June 2020 to May 2022. We used data from September 2022 as the validation dataset and data from August 2022 as the test dataset. We pre-trained the model on data from June 2020 to May 2022; we excluded data from the winter season and the validation and test datasets. During training, we used only data containing precipitation to ensure stability. During the model training, we utilized the cell-linked list method to remap RDAPS data at a 3-km resolution to QPE data at a 5-km resolution [10]. We used z-scores to normalize all variables. Additionally, for variables with the same attributes but different vertical levels, separate normalization was applied. We extracted data for the Korean Peninsula only and resized them to dimensions of  $224 \times 128$ .

**Metnet.** Sonderby et al. (2020) proposed Metnet [22] for precipitation nowcasting. Metnet uses a ConvLSTM that employs an attention mechanism. Moreover, Kim et al. (2022) used Metnet for a precipitation post-processor [11] that outperformed other architectures. We used the Metnet architecture and propose its use as a precipitation post-processor. The code and data are publicly available <https://github.com/osilab-kaist/KoMet-Benchmark-Dataset>. For the model validation, we set the window size to three and the learning rate to 3e-03. The optimizer was AdamW [13] with  $\beta_1$  and  $\beta_2$  set to 0.9 and 0.999, respectively.

**Ours.** Our encoder employs an InternImage [23] architecture. The proposed model uses a spatiotemporal masking method. We set a spatial patch size of  $16 \times 16$  and temporal patch size of  $4 \times 4$ . We set the loss weight of the cross-entropy to  $w_i = 1, 5, 10$ . For a  $16 \times 224 \times 128$  input, the patch size was  $4 \times 14 \times 8$ . Our pre-training configuration follows that presented in [23]. Table 3 details the configurations we used.

Table 3: Hyperparameters setting.

Config	Pre-training	Training
optimizer	AdamW [13]	AdamW [13]
optimizer momentum	$\beta_1, \beta_2=0.9, 0.95$	$\beta_1, \beta_2=0.9, 0.999$
weight decay	0.05	-
learning rate	1.6e-3	1e-4
learning rate schedule	cosine decay [12]	-
warmup epochs [7]	120	-
epochs	1000	200
batch size	64	32
gradient clipping	0.02	-

## D Additional Experimental Results

### D.1 Ablation on mask ratio

To determine the optimal masking ratio for precipitation correction, we compared the masking ratio results during pre-training and transfer learning. Tables 4 and D.1 show that the larger the masking ratio in the pre-training, the better the results. Conversely, the smaller the masking ratio in transfer learning, the better the results.

Table 4: Results on mask sampling in pre-training.

Mask ratio	CSI (0.1)	CSI (10)
50%	0.310	0.088
75%	0.320	<b>0.090</b>
90%	<b>0.322</b>	0.089

Table 5: Results on mask sampling in transfer learning.

Mask ratio	CSI (0.1)	CSI (10)
0%	0.318	0.083
25%	<b>0.347</b>	<b>0.093</b>
50%	0.322	0.086

### D.2 Ablation study on lead time

The precipitation data of the NWP model were extracted and trained by extracting 25–30 forecasts for post-processing with a 24-h lead time. In the training, the lead time was not considered. However, as shown in Figure 3, the accuracy was measured to understand the degree of the CSI improvement based on the lead time. Figure 5 shows that the overall precipitation data were corrected regardless of the lead time, and the improvement was approximately 39.49% for the 27-h forecast data. The results show that the proposed model is effective for precipitation correction and robust to error correction, owing to the lead time.

### D.3 Points of interest

Zhou et al. [26] proposed a methodology for computing class-discriminative activation maps. The method employs a novel set of weights trained separately for each feature map in the context of image

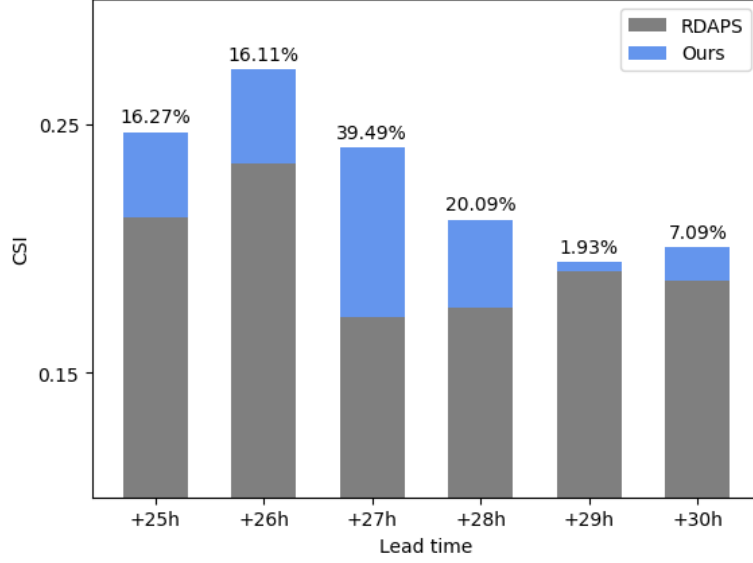


Figure 5: Bar plots by lead time. Scores with a CSI of 0.1 or higher and scores with a CSI of 10 or higher are averaged across lead times, and the improvement over RDAPS is shown in percentage.

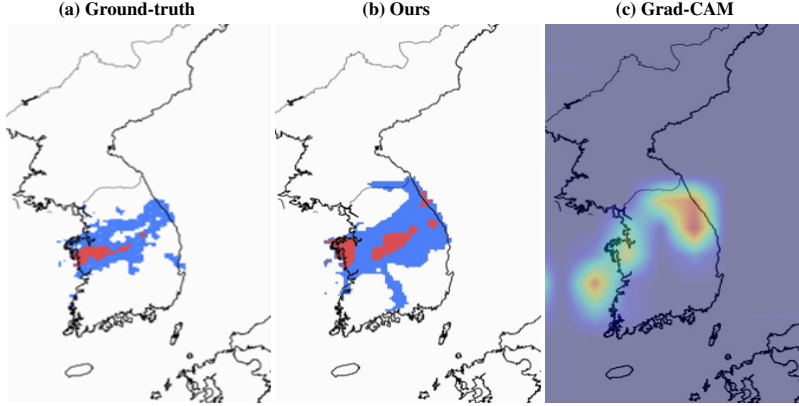


Figure 6: Heat map visualization at the depth selected for the test case: (a) Ground truth data; (b) segmented results; (c) heat map superimposed on top of the original image. In GradCAM maps, warmer colors indicate a higher pixel contribution to the correct prediction, while cooler colors signify a lower contribution.

classification tasks. The class activation map is obtained as follows:

$$M_{i,j}^c = \sum_{k=1} \omega_k^c m_{i,j}^k, \quad (3)$$

where  $m_k$  is the  $k$ -th feature map of the final convolution layer, and the weights  $\omega_k^c$  are trained separately with global average pooling and individual feature maps  $F_k = \sum_i \sum_j m_{i,j}^k$ . The score of class  $S_c$  is the sum of all class activation maps,  $S_c = \sum_i \sum_j M_{i,j}^c$ . Grad-CAM [19] is a natural progression of the original CAM implementation, which eliminates the necessity of training a fresh set of weights. Instead, the weight  $\omega_k^c$  for a certain class  $c$  can be calculated as

$$\omega_k^c = \sum_i \sum_j \frac{\partial S^c}{\partial m_{i,j}^k}. \quad (4)$$

Figure 6 shows a heatmap of the visualization parts that the model focuses on, based on the case compared in Figure 4.